Dual Mode Redox-Responsive MRI Contrast Agents

by

Hillary Rose Polander

A thesis submitted to the Graduate Faculty of
Auburn University
In partial fulfillment of the
requirements for the Degree of
Master of Science

Auburn, Alabama
August 6, 2022

Approved by

Christian R. Goldsmith, Chair, Professor of Chemistry and Biochemistry
Evert Duin, Professor of Chemistry and Biochemistry
Wei Zhan, Professor of Chemistry and Biochemistry
Ethan Hill, Assistant Professor of Chemistry and Biochemistry

Abstract

Magnetic resonance imaging (MRI) contrast agents function by shortening the relaxation times of targeted nuclei, thereby better distinguishing regions with different local concentrations of the visualized nuclei. Drawbacks with responsive T_1-weighted (T_{1w}) MRI contrast agents, such as high background signal, has led to the investigation of dual-mode imaging. With paramagnetic contrast agents for both ^{1}H and ^{19}F MRI, the identity and oxidation state of the metal influence the relaxivities. Since the signals of both modes are connected to the oxidation state of the metal center, they can be used to detect biologically aberrant redox behavior, such as that associated with neurological disease. This project aimed to extend the laboratory's prior successes in redox-responsive MRI contrast agents to bimodal sensors with ^{1}H and ^{19}F MRI outputs.

Table of Contents

List of Tables

List of Figures

List of Equations

List of Schemes

Chapter 1: Introduction

1.1. Fundamentals of Magnetic Resonance

Magnetic resonance imaging (MRI) can non-invasively visualize soft tissue within the body.[1] The MR instrument applies a static magnetic field (B_0) at the subject which causes nuclei to align to the applied external field. The net magnetization vector of these nuclei rotates around the B_0 axis where the frequency of rotation, known as the Larmor frequency, is proportional to the field strength.[2,3] The Larmor equation is shown in **Equation 1.1** where ω_o = Larmor frequency, γ = the gyro magnetic ratio of the nucleus of interest, and B_0 = field strength.

$$\omega_o = -\gamma B_0 \tag{1.1}$$

The nuclei under investigation can then be tipped out of alignment with the static field by means of a perpendicularly applied radiofrequency pulse (RF) that matches the Larmor frequency.[3] Atomic nuclei that can be visualized include, but are not limited to, the hydrogen nucleus (^{1}H) and fluorine nucleus (^{19}F). The former is the most frequently used within current medical applications.

As the nuclei relax and return to their original magnetization equilibrium, a secondary echo RF signal is detected and converted into an image.[4] The amount of energy released and the time it takes for the nuclei to return to the alignment of B_0 contributes to the intensity of the echo signal. The faster the realignment, known as relaxation, the greater the signal intensity.

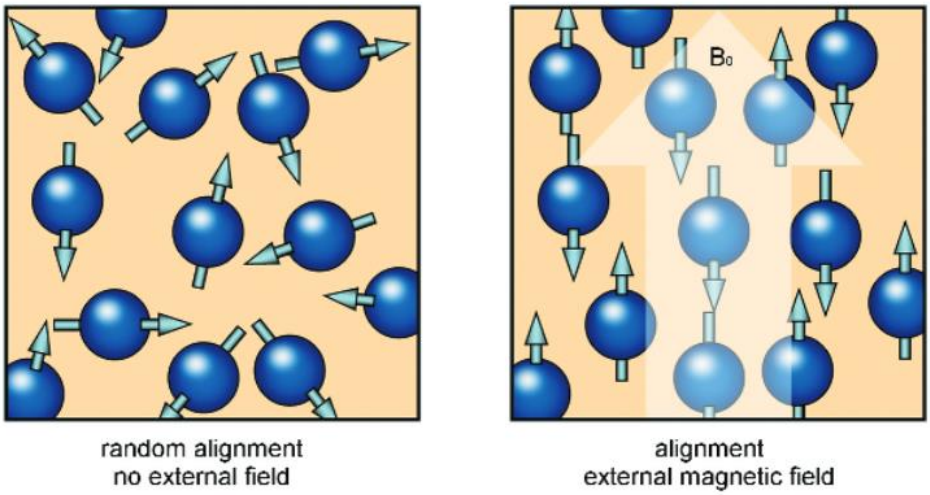

Figure 1.1. After the application of a magnetic field B_0, lower energy (spin-up) ^1H nuclei align parallel to B_0 while higher energy ^1H nuclei align anti-parallel to B_0. This figure was taken from reference 3 and reproduced with permission from John Wiley and Sons.

1.2. MRI Signal Fundamentals

Soft tissues are usually discerned from one another in ^1H-based MRI studies on the basis of their water content.[5] The signal intensity largely depends on the longitudinal relaxation rate ($1/T_1$) and the transverse relaxation rate ($1/T_2$) of the water protons.[6] The T_1 relaxation constant corresponds to the time needed for 63% of the magnetization moment M_z to return to its original alignment with the static field, whereas the T_2 relaxation constant is the time needed for 37% of the magnetization moment M_{xy} to decay to its original value (**Figure 1.2** and **Figure 1.3**).[7]

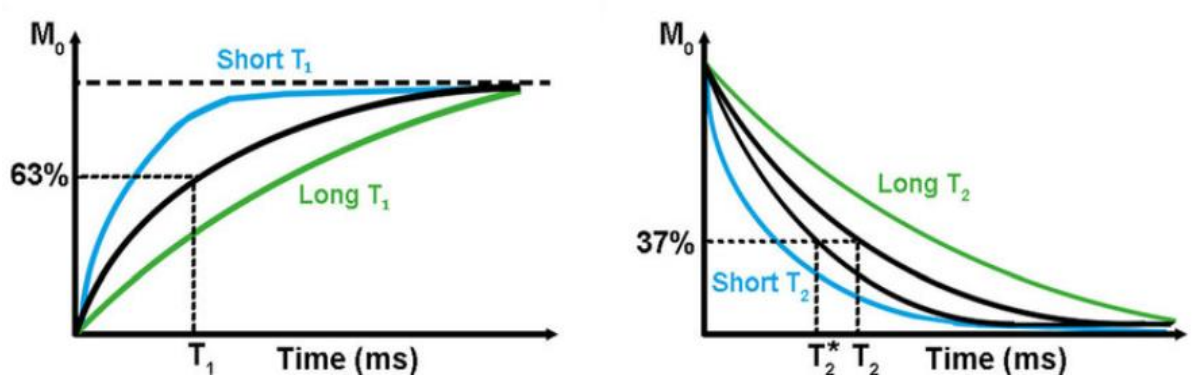

Figure 1.2. *T_1* relaxation (left) and *T_2* relaxation (right) illustration of tissues with short (blue) and long (green) *T_1* values. *T_2** is the observed value while *T_2* is the true value. The figure was taken from reference 7 and reproduced with permission from Springer Nature.

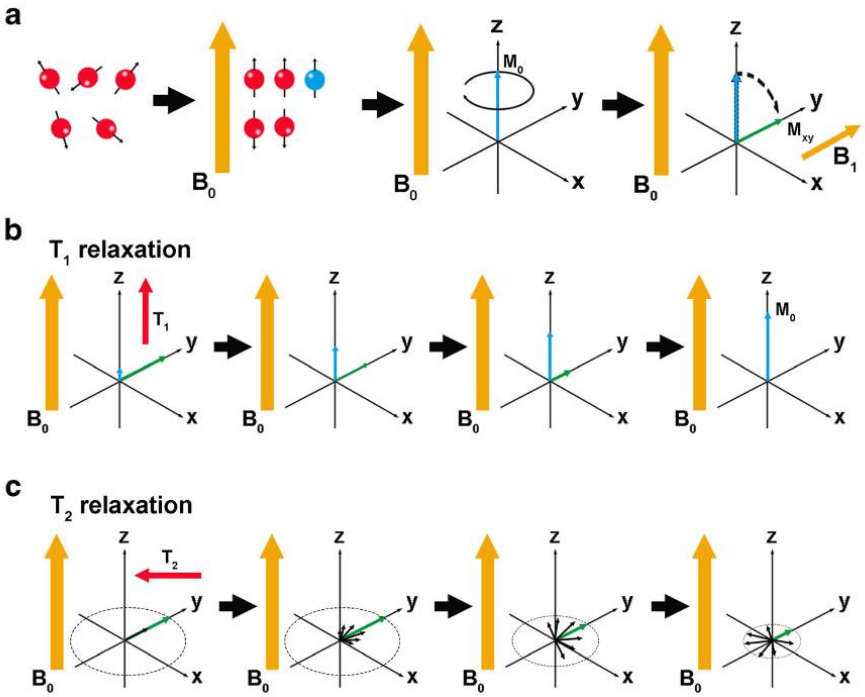

Figure 1.3. Schematic representation of ^{1}H nuclei relaxation pathways. **A)** When an external magnetic field (B_0) is applied, protons align parallel or antiparallel to the direction of that field. The sum of those protons is expressed as a magnetization vector (M_0). A second magnetic field (B_1) is applied perpendicular to B_0 and the nuclei tilt into the x-y plane. Once B_1 is switched off, the ^{1}H nuclei relax back to their original alignment through **B)** *T_1* relaxation or **C)** *T_2* relaxation. This figure was taken from reference 7 and reproduced with permission from Springer Nature.

The signal typically increases with increasing $1/T_1$ and decreases with increasing $1/T_2$. However, the identities of the contrast agent and the specific RF pulse sequences can be used to

selectively enhance changes in either $1/T_1$ or $1/T_2$, which are known as T_1-weighted (T_{1w}) and T_2-weighted (T_{2w}) scans, respectively.[6]

1.3. T_1-Weighted Contrast Agents

In some cases, ^{1}H MRI by itself does not sufficiently differentiate tissues as shown in **Figure 1.4**.[8] Here, two T_{1w} scans of a mouse brain were taken with and without an injected contrast agent. A tumor within the brain is visualized only when the contrast agent is added. Contrast agents function by shortening the relaxation times of targeted nuclei, thereby better distinguishing regions with different local concentrations of the visualized nuclei.[9] The longitudinal and transverse relaxivities, r_1 and r_2, refer to the amount of increase in $1/T_1$ and $1/T_2$, respectively, per millimolar (mM) of contrast agent.[11] Small molecule contrast agents typically produce a larger percentile change in T_1; since the end-goal of this research is to prepare small molecule MRI contrast agents, this chapter will focus almost exclusively on this value. One benefit of T_{1w} contrast agents is that the image becomes sharper due to the enhanced contrast as the relaxivity increases. The r_1 value of a compound is therefore the primary measure of its effectiveness as a T_1-weighted relaxation agent.[10]

Contrast agents can be either paramagnetic or super-paramagnetic. The small molecule paramagnetic compounds shorten T_1 relaxation times to improve the image. Super-paramagnetic contrast agents, conversely, are magnetic nanoparticles (SPMNPs) that more strongly effect T_2.[12] This thesis will focus on the former class, which is mostly comprised of Gd(III) complexes.

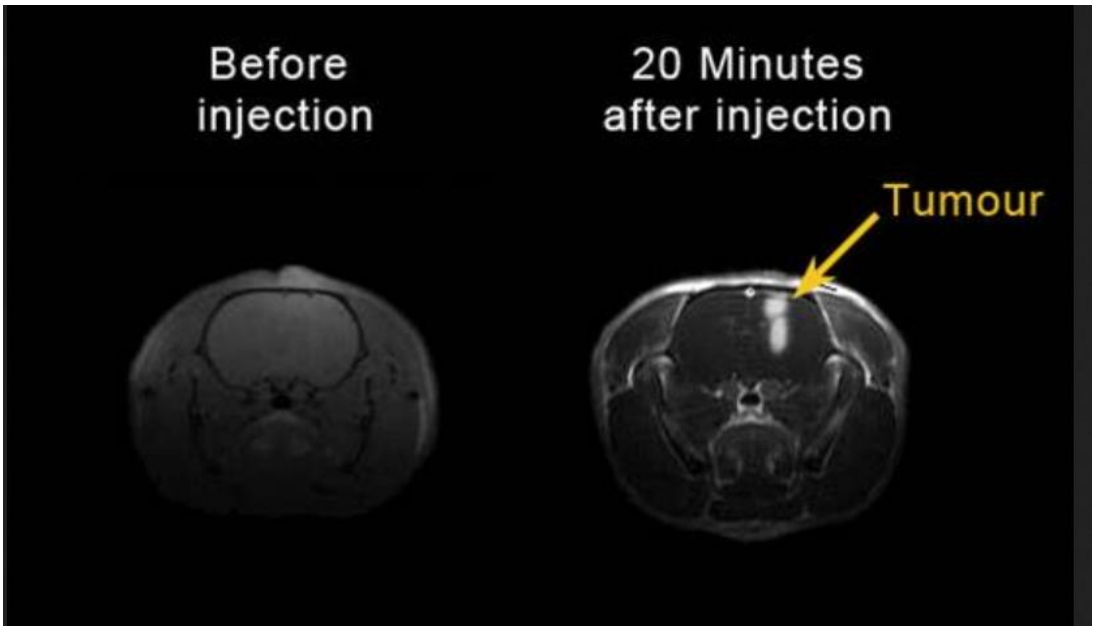

Figure 1.4. A contrast agent enables the visualization of a brain tumor that was previously undetectable. Figure taken from reference 8 and reproduced with permission from the American Chemical Society.

Gd(III)-containing complexes are the most widely used T_1 shortening agents in clinical medicine today.[13] Gd(III) is highly paramagnetic due to its seven unpaired electrons. Although a large number of Gd(III) complexes have been used in the clinic, they have drawbacks that have motivated the search for alternative classes of contrast agents. One notable drawback is the high *in vivo* toxicity of the "free" Gd(III) ion, which is actually aquated $[Gd(H_2O)_8]^{3+}$. In order to avoid this toxicity, the metal ion needs to be complexed to a strongly chelating organic molecule before being administered to a patient; the high denticity of these ligands leaves few accessible coordination sites for water.[14] This in turn attenuates the ability of the contrast agent to interact with water molecules and worsens the relaxivity (*vide infra*). In order to compensate for the low r_1 values, these complexes need to be administered in high doses to impact the signal. Additionally, it is only possible to image areas where the contrast agent accumulates, notably the blood stream.[14] Current work in the field aims to both improve the relaxivities and to develop the means to target

specific tissues or organs within the body; both measures would reduce the necessary dose of the contrast agent.

The r_1 of a contrast agent depends on inner-sphere, outer sphere, and second-sphere interactions with bulk water molecules (**Figure 1.5**).[5] Modifying the inner-sphere component (r_{1IS}) of the complex is the most synthetically straightforward approach.

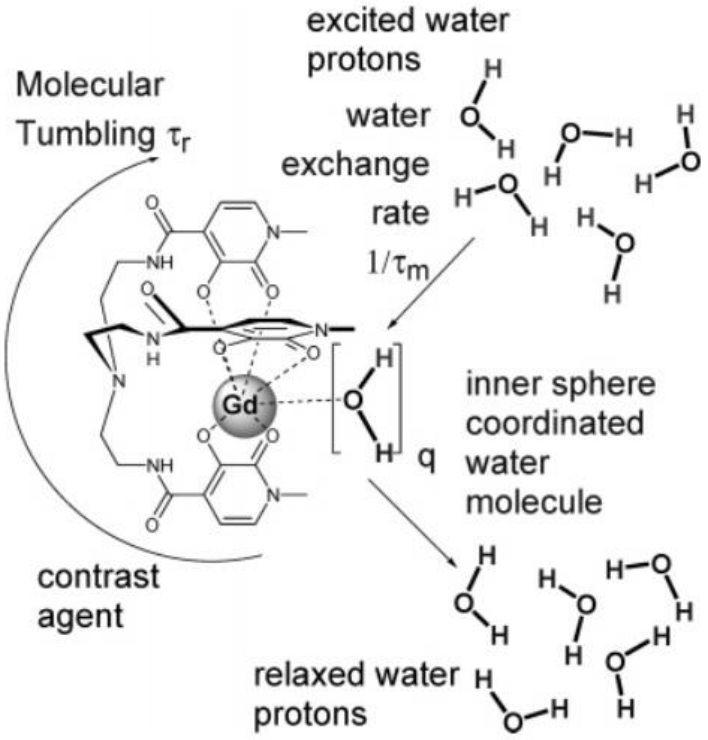

Figure 1.5. Conditions influencing relaxivity. The electron spin of the paramagnetic metal center and the interaction it has with the nuclear spin of the bound water molecule give rise to the inner-sphere component. Interactions with adjacent water molecules are responsible for the outer-sphere component. This graphic is from reference 14 and reproduced with permission from the American Chemical Society.

As shown in **Equation 1.2**, the inner-sphere relaxation time constant is dependent on the aquation number of the metal center (q), the relaxation time (T_{1m}), and the mean occupancy time (τ_m) of the coordinated water molecules.

$$r_{1IS} = \frac{q/_{[H2O]}}{T1m + \tau m} \qquad (1.2)$$

The relaxivity of a Gd(III)-based contrast agent can be improved by either allowing a greater number of inner-sphere water molecules to coordinate (q), shortening the water residence time (τ_m), or slowing the molecular tumbling rate ($1/\tau_r$).[14] With respect to tuning q, this is normally done by altering the denticity of the organic ligand; less highly chelating ligands allow more coordination sites for water on the metal ion. Unfortunately, as the denticity decreases, the water-stability of the contrast agent worsens. In practice, it is difficult to obtain a q above 2 without the Gd(III) dissociating from the ligand and causing biological harm.

The identity of the metal ion has a great influence on the T_1 relaxation time constants. Generally, more paramagnetic ions lead to shorter relaxation times, and therefore larger r_{1IS}. Electron-spin relaxation is another important factor that relates to the specific metal ion.[15] Some highly paramagnetic metal ions, such as high-spin Fe(II), will be inadequate for T_{1w} imaging due to their fast electron spin relaxation times. Mn(II), Fe(III), and Gd(III), conversely, have slow electron spin relaxation times. Since all three of these are also highly paramagnetic (S = 5/2 or 7/2), they are ideal for use in T_{1w} MRI contrast agents.

1.4. MRI Contrast Agent Sensors

An MRI scanner normally provides morphological information, but details about biochemical processes within the body can potentially be obtained with a smart or responsive MRI contrast agent.[21] The underlying concept is that the relaxivity of the contrast agent changes upon reaction with a particular analyte, such as an enzyme or a metal ion. With a "turn-on" sensor, the relaxivity increases upon the reaction, resulting in sharper contrast in regions where the analyte is present. Responsive molecular magnetic resonance imaging probes have been designed to report

on biomarkers such as biologically relevant cations, anions, pH, enzymatic activity, and redox homeostasis.[21,26]

In practice, however, it is difficult to discern if enhanced contrast with a turn-on sensor results from the activation of the probe or merely the accumulation of its lower relaxivity form. Ideally, a turn-on contrast agent should give little to no signal upon administration and remains "off" until it has reached its target, upon which turns "on" and provides a strong signal.

1.5. Reactive Oxygen Species

During regular cellular metabolism, reactive oxygen species (ROS), such as H_2O_2, $O_2^{\bullet-}$, and HO•, are produced in small quantities.[30] Of all the biological processes that produce ROS, complexes I and III of the mitochondria are the largest contributors, producing H_2O_2 and $O_2^{\bullet-}$ during oxidative phosphorylation.[16] Accumulation of these species are strictly curtailed in healthy organisms by antioxidant enzymes such as superoxide dismutase (SOD, **Figure 1.6**), which catalyzes the dismutation of $O_2^{\bullet-}$ into the less damaging H_2O_2.[17,18] Catalases then convert the generated H_2O_2 in the body to O_2 and water. Over-accumulation of ROS leads to oxidative stress, which has been identified as a factor in both aging and the progression of several neurological disorders such as Alzheimer's disease (AD).[19] In the early stages of AD, levels of oxidized proteins and lipid peroxidation were found to be elevated, suggesting a link between oxidative stress and AD.[19]

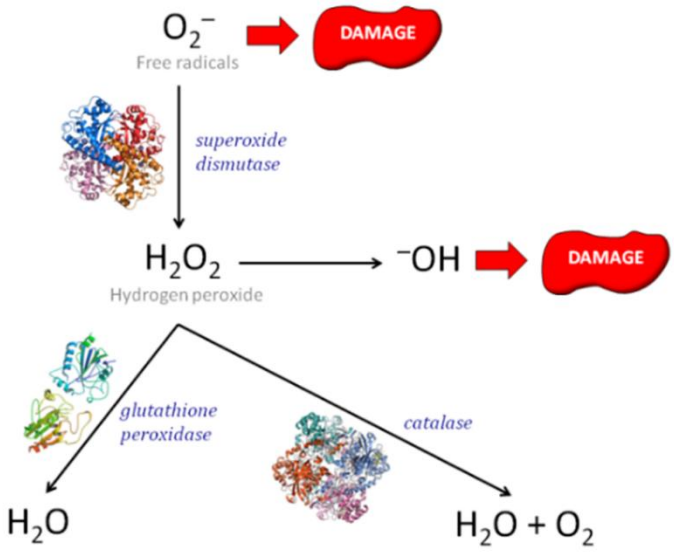

Figure 1.6. Simple schematic of SOD and catalase mechanism. The figure was taken from reference 17 and reproduced with permission from Science and Education Publishing.

To better understand the connections between ROS and disease progression, we need more selective imaging techniques that can discern healthy from irregular redox activity.[19] Due to its ability to non-invasively probe tissues and organs, MRI is highly attractive, and the use of a smart contrast agent that can respond to aberrant redox activity could allow MRI to detect hotspots of oxidative stress within the body. With respect to which specific ROS to target, H_2O_2 is arguably the best target since it is believed that this oxidant accumulates at higher concentrations than other ROS.[27]

1.6. Redox-Responsive Contrast Agents

When designing a redox-activatable contrast agent, there are several parameters that must be met for it to be effective *in vivo*. These include: A) a large change in signal between the "on" and "off" states, B) low baseline relaxivity for the "off" state, C) a fast rate of reactivity with the target ROS, D) high aqueous stability of the probe in both its "on" and "off" states, E) sufficient

aqueous solubility, and F) low toxicity.[22] With respect to the underlying reaction with the ROS, either the metal ion or the organic ligand need to be able to react. This makes it difficult to use Gd(III) for such applications since gadolinium is only stable in the +3 oxidation state.

I will discuss one recent successful H_2O_2 probe in more detail. Wang et al. reported that the complex Fe-PyC3A (**Figure 1.7**) displayed a higher r_1 upon reaction with H_2O_2.[22] The underlying design is that the preactivated sensor is an Fe(II) species, which is a poor T_{1w} relaxation agent, but the activated form contains high-spin Fe(III), which is a very strong T_1 relaxation agent.[22] The reaction with H_2O_2 oxidizes the metal ion and increases MRI contrast. **Table 1.1** provides the relaxivities measured for the sensor in both its Fe(II) and Fe(III) forms. The Fe(II) complex has such a low relaxivity that the signal change is negligible at concentrations as great as 0.5 mM. Oxidation to the Fe(III) form results in an order of magnitude increase in r_1; unfortunately, this is still a relatively low value that is below the 3-4 mM^{-1} s^{-1} for a typical Gd(III)-containing contrast agent. Nonetheless, Wang et al. were able to use their contrast agent to image inflammation in a mouse pancreas (**Figure 1.8**).

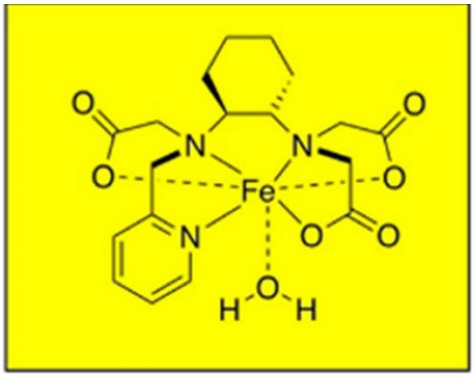

Figure 1.7. Structure of Fe(III)/(II)-PyC3A. The graphic is from reference 22 and reproduced with the permission from the American Chemical Society.

Table 1. Relaxivity of Fe^{3+}- and Fe^{2+}-PyC3A Recorded in pH 7.4 Tris Buffer at 1.4, 4.7, and 11.7 T

	r_1Fe^{3+}-PyC3A ($mM^{-1}s^{-1}$)	r_1Fe^{2+}-PyC3A ($mM^{-1}s^{-1}$)	r_1Fe^{3+}/r_1Fe^{2+}
1.4T[a]	1.8 ± 0.1	0.18 ± 0.01	10.0
4.7T[b]	2.4 ± 0.4	0.18 ± 0.01	13.3
11.7T[a]	2.2 ± 0.1	0.15 ± 0.01	14.5

[a]Recorded at 37 °C. [b]Recorded at room temperature.

Table 1.1. Relaxivity results reported by Wang et al. Table taken from reference 22 and reproduced with permission from the American Chemical Society.

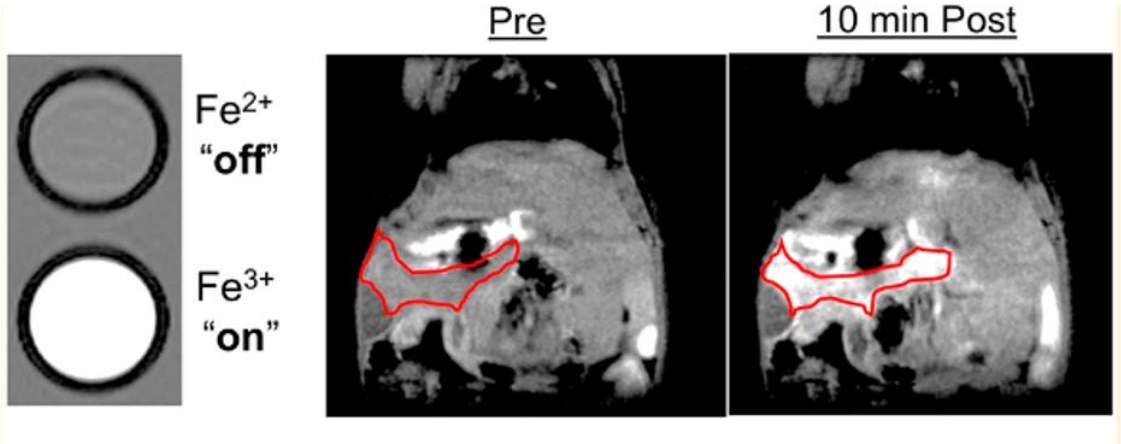

Figure 1.8. Imaging results of inflamed mouse pancreas tissue using Fe(III)/(II)-PyC3A redox-activatable MRI contrast agent. After oxidation by H_2O_2 to high spin Fe(III), strong and selective imaging enhancement is observed. The figure is from reference 22 and reproduced with the permission from the American Chemical Society.

1.7. ^{19}F MRI

One issue with responsive T_{1w} MRI contrast agents is that both the water and the preactivated sensor normally provide a high background signal. Even with the sensor reported by Wang et al., the water by itself contributes substantially to the image (**Figure 1.8**).[22] This issue has motivated many to investigate ^{19}F as an alternative nucleus to ^{1}H. The primary advantage of ^{19}F probes over ^{1}H MRI contrast agents is that there is very little imageable fluorine within the body, resulting in a negligible background signal.[23] To a first approximation, the only fluorine that is

present is that provided by the contrast agent. ^{19}F MRI data are relatively easy to acquire on a traditional ^{1}H MRI scanner; one only needs an additional specialized radiofrequency coil. Another benefit to ^{19}F MRI is that the nuclei have resonance frequencies over a large chemical shift range (>300 ppm) which allows for distinct resonances to be independently imaged if they are sufficiently separated. Fluorine nuclei also have very short transverse relaxation times (T_2) that give rise to very broad signals that can be easily resolved with appropriate pulse sequences.

Unlike ^{1}H MRI, ^{19}F MRI absolutely requires a contrast agent. Both organic and inorganic molecules have been investigated for this application. Relative to ^{1}H MRI, larger concentrations of the ^{19}F-containing contrast agent are normally needed to see a strong signal, although this requirement can be alleviated somewhat by installing multiple chemically equivalent fluorine atoms onto the contrast agent.[23] Paramagnetic metal ions can potentially improve the signal intensity by shortening T_1 relaxation times. Unfortunately, one cannot weight ^{19}F MRI contrast agents towards T_1 as is frequently done with ^{1}H MRI contrast agents; one must also consider T_2. To optimize signal intensity, one must reduce T_1 as much as possible while minutely effecting T_2, which would achieve a T_2/T_1 value near 1. The sensitivity of fluorine probes is therefore proportional to the T_2/T_1 ratio, not just the effective magnetic moment (μ_{eff}).

Srivastava et al. reported a fluorinated Fe(II) complex that can act as a ^{19}F MRI probe.[24] The advantages to using a coordination complex over a diamagnetic contrast agent included higher water solubility and a strong fluorine NMR signal with short T_1 relaxation times. Fluorinated Fe(II) complexes have a much higher sensitivity than other first-row transition metal ions as well as paramagnetic lanthanides.[25] As will be further discussed in Chapter 2, the design of the fluorinated ligand along and the selection of the paramagnetic metal center are key factors for tuning the relaxation times and signal intensities.

The macrocycle DOTAm-F12 (**Figure 1.9**) was complexed to a variety of metals in addition to Fe(II): La(III), Eu(III), Gd(III), Tb(III), Dy(III), Ho(III), Er(III), Tm(III), and Yb(III).[25] The complexes were then assessed as ^{19}F MRI contrast agents. The twelve chemically equivalent fluorine nuclei on the DOTAm-F12 ligand result in a strong signal for most of the metal ions (**Figure 1.10**).

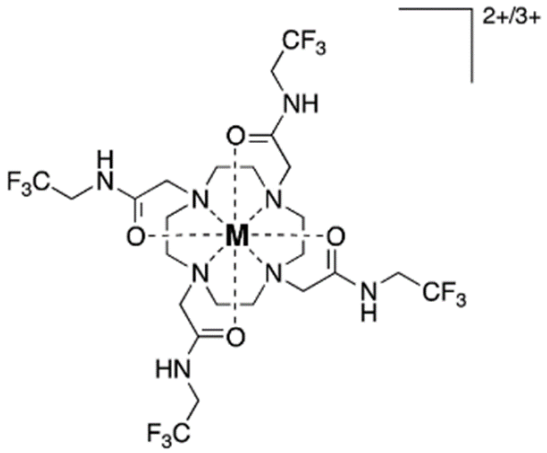

Figure 1.9. Structure of M-DOTAm-F12 where M = La(III), Eu(III), Gd(III), Tb(III), Dy(III), Ho(III), Er(III), Tm(III), Yb(III), and Fe(II). The graphic is from reference 25 and reproduced with permission from the American Chemical Society.

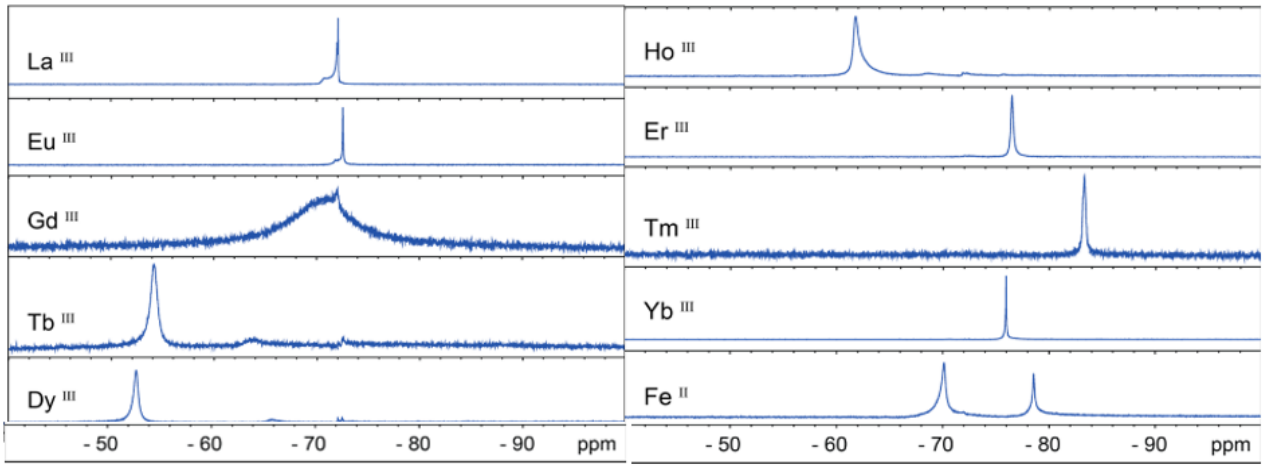

Figure 1.10. ^{19}F NMR spectra of the M-DOTAm-F12 complexes in D_2O. Each complex gave rise to a single peak. In the Fe(II) spectrum, the peak at −78.6 ppm corresponds to the trifluoromethanesulfonate counterion. The broadened peak for Gd(III) results from the shortening of T_2. If T_2 becomes too short, the signal is broadened to the point that it cannot be visualized. This graphic is from reference 25 and reproduced with permission from the American Chemical Society.

The shorter T_1 allows for more scans to be obtained within a set time, increasing the sensitivity. As seen in **Table 1.2**, Fe(II) has the best T_2/T_1 ratio, followed by Ho(III). Although Gd(III) is excellent for T_{1w} ^{1}H MRI, it does not support ^{19}F MRI. When comparing Fe(II) to Gd(III), the improved T_2/T_1 ratio is even more pronounced. The relaxation constants depend heavily on the environment and better T_2/T_1 ratios are seen in water as opposed to rat blood.

^{19}F T_1 and T_2 Relaxation Times, T_2/T_1 Ratio, and MRI SNR of Select M-DOTAm-F12 Complexes in Rat Venous Blood at 37 °C

	T_1[a] (ms)	T_2[a] (ms)	T_2/T_1[a]	SNR[b,c]
La-DOTAm-F12	700	29	0.041	n.d.
Ho-DOTAm-F12	10	2.7	0.26	~1[d]
Tm-DOTAm-F12	36	6.4	0.18	10
Yb-DOTAm-F12	170	12	0.071	6.1
Fe^{II}-DOTAm-F12	7.7	4.4	0.57	16.3

T_1 and T_2 Relaxation Times, and MRI SNR of M-DOTAm-F12 Complexes in Water at B_0

	T_1[d] (ms)	T_2[d] (ms)	T_2/T_1[d]	SNR[fg]
La-DOTAm-F12	570	400[h]	0.70	4.7
Eu-DOTAm-F12	360	41[h]	0.11	6.6
Gd-DOTAm-F12	12	0.14[i]	0.01	~1
Tb-DOTAm-F12	6.3	1.3[h]	0.21	6.5
Dy-DOTAm-F12	5.9	2.2[h]	0.37	6.6
Ho-DOTAm-F12	7.6	5.4[h]	0.71	32
Er-DOTAm-F12	14	8.8[h]	0.63	14
Tm-DOTAm-F12	26	16[h]	0.61	20
Yb-DOTAm-F12	130	55[h]	0.42	23
Fe^{II}-DOTAm-F12	5.7	5.6[h]	0.98	28

Table 1.2. M-DOTAm-F12 relaxivity results in blood and water where [M-DOTAm-F12] = 5 mM. The Fe(II) species provides the T_2/T_1 ratio closest to unity in both mediums. Magnetic resonance images of samples in water and in blood were measured at 33°C using a 9.4-T, 31-cm horizontal bore magnet. B_0 = 7.0 T (rat venous blood).This graphic is from reference 25 and reproduced with permission from the American Chemical Society.

Conclusion

With both ^{1}H and ^{19}F MRI, the identity and oxidation state of the metal influence the relaxivities and thereby the signal-to-noise ratios. Both modes of MRI can be used to detect biologically relevant redox behavior since the signals are both connected to the oxidation state of the component metal ion.

Chapter Two: Design and Characterization of [Fe(Ftris)(ClO_4)$_2$]

2.1. Introduction

My graduate work was directed towards developing a redox-responsive bimodal MRI contrast agent. This would be comprised of a fluorinated ligand that would be initially complexed to Fe(II). Such a compound should have a strong ^{19}F MRI signal but have a negligible impact on the ^{1}H MRI image. Oxidation by H_2O_2 would convert the ferrous complex to an Fe(III) species. This is anticipated to either severely attenuate or eliminate the ^{19}F MRI signal while increasing the T_1-weighted relaxivity enough to cause a detectable change in the ^{1}H MR image.

We further envision using a redox-active ligand to improve the ^{1}H MRI response by introducing water coordination sites in the Fe(III) product. This can be done by using a ligand that gets oxidized to a less highly chelating form. Recently, the Goldsmith group has prepared a number of manganese and iron compounds with quinol-containing ligands, such as H_2qp1 (**Figure 2.1**).[10,27] In water, the quinols readily deprotonate to quinolate ions and coordinate strongly to positively charged metal ions. Upon oxidation by H_2O_2, the quinols convert to *para*-quinone groups which act as poor ligands. Water molecules can displace the *para*-quinones, increasing both q and r_1. With these compounds, a redox-active transition metal ion is needed to serve as both the paramagnetic reporter and the catalyst for the oxidation of the organic ligand.

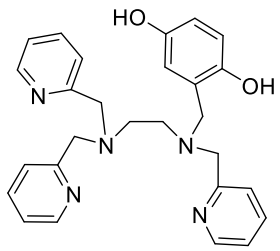

Figure 2.1. Structure of *N*-(2,5-dihydroxybenzyl)-*N*,*N*′,*N*′-tris(2-pyridinylmethyl)-1,2-ethanediamine (H_2qp1).[10]

My goal was to prepare fluorinated versions of previous polydentate quinol-containing ligands that were developed for Mn(II)-containing MRI contrast agents and then synthesize complexes with the fluorinated molecules to Fe(II). The initial target is a fluorinated version of H_2qp1.

2.2. Experimental

Materials

All chemicals and solvents were purchased from Sigma-Aldrich and used as received unless otherwise noted. All deuterated solvents were bought from Cambridge Isotopes. Diethyl ether (ether) and methanol (MeOH) were bought from Fisher. The synthesis of *N*-(2,5-dihydroxybenzyl)-*N,N′,N′*-tris(2-pyridinylmethyl)-1,2-ethanediamine (H_2qp1) was previously described and used as basis for the syntheses of both the fluorinated analogue F_3H_2qp1 and fluorinated trispicen (FTris).[10,27]

Instrumentation

^{1}H and ^{19}F nuclear magnetic resonance (NMR) data were taken on a 500 MHz AV Bruker NMR spectrometer at 294 K in either MeCN-d3 or D_2O. In each spectrum, the reported NMR resonance peak frequencies were referenced to internal standards. A Varian Cary 50 spectrophotometer was used to collect optical data. High-resolution mass spectrometry (HR-MS) data were collected at the Mass Spectrometer Center at Auburn University on a Bruker microflex LT matrix-assisted laser desorption ionization time-of-flight (MALDI-TOF) mass spectrometer via direct probe analysis operated in the positive-ion mode. Solid samples of the Fe(II) complex were dried, stored under N_2, and sent to Atlantic Microlabs (Norcross, GA) for elemental analysis.

Synthesis of Fluorinated Trispicen

Two equiv. of 5-fluoro-2-formylpyridine (0.5 g, 0.003 mol) were combined with 140 μL of ethylenediamine in 20 mL of MeOH and was allowed to stir for 1 h. At this point, 2.6 equiv. of $NaBH_4$ (0.2 g, 0.005 mol) were slowly added, and the reaction mixture stirred overnight. The solvent was removed by rotavaporation, and the crude product was extracted with CH_2Cl_2. The extracts were washed with 0.2 M KOH, dried with Na_2SO_4, and concentrated to a yellow oil, which was determined to be compound **1** (**Scheme 2.1**). The compound's identity was confirmed with ^{1}H NMR (**Figure S6**), ^{13}C NMR (**Figure S7**), and mass spectrometry (**Figure S8**). The average percent yield of the reaction was 63%.

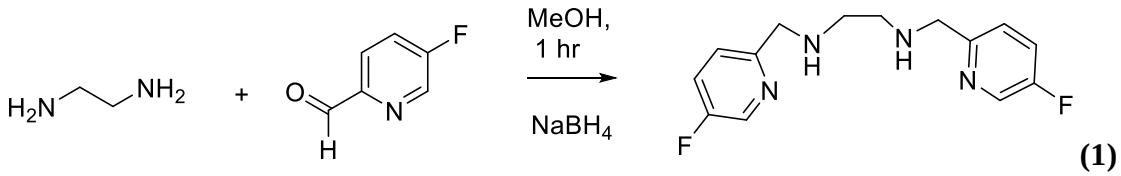

(1)

Scheme 2.1. First step in the synthesis of FTris.

Compound **1** and 1 equiv. of 5-fluoro-2-formylpyridine were dissolved in 10 mL of ether and stirred overnight at room temperature. The solvent was removed through rotavaporation. The crude was dissolved in a minimal amount of ether and then stored in the freezer. This deposited the product **2** as a chunky, white precipitate **(Scheme 2.2)**. The precipitate was taken directly to the last step of the synthesis and was not characterized.

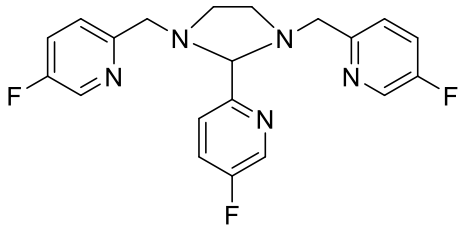

(2)

Scheme 2.2. Expected product from the second step in the synthesis of FTris.

Compound **2** and 2.4 equiv. of trifluoroacetic acid were dissolved in MeOH and stirred for 30 min. At this point, 1.2 equiv. of $NaBH_3CN$ were added to the reaction mixture, and the solution stirred overnight. The reaction was quenched with 4 M NaOH solution. At this point, the crude product was extracted with CH_2Cl_2. The extracts were dried over Na_2SO_4 and concentrated to yield the FTris product (**Scheme 2.3**). ^{1}H NMR (**Figure S1**), ^{19}F NMR (**Figure S2**), and mass spectrometry (**Figure S3**) were taken before storing FTris under nitrogen. The average percent yield of the reaction is 47%.

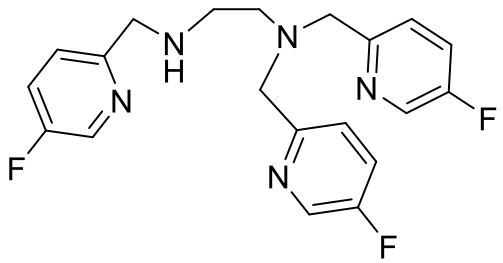

Scheme 2.3. Structure of FTris.

Complexation of FTris to Fe(II)

FTris (52 mg, 0.13 mmol) and [$Fe^{II}(ClO_4)_2$] (35 mg, 0.12 mmol) were dissolved in 2 mL of MeCN under N_2. The solution stirred overnight. Ether was gradually added in an attempt to precipitate the product. After two days, a sticky red precipitate was obtained; this was dried over vacuum to yield 0.014 g of product. The ^{19}F NMR spectrum was taken in MeCN-d_3 (**Figure S4**).

Elemental Analysis: Calculated for $Fe(C_{20}H_{20}F_3N_5)(ClO_4)_2$: C, 37.41%; H, 3.14%; N, 10.91%; Found: C, 36.96%; H, 3.56%; N, 11.95%.

2.3. Results and Discussion

A number of fluorinated analogues of H_2qp1 can be made by introducing fluorinated starting materials into the previously reported synthesis.[10,27] Although the fluorine atoms could be installed on either the quinol or pyridine groups, my work focused on fluorinating the pyridine rings.

Prior work suggested that the placement of fluorine atoms (F or CF_3) 5-7 Å away from the Fe(II) center will maximize the ^{19}F MRI signal.[28] To ensure this, the F or CF_3 should be placed on the 4- and 5- positions of the pyridine ring. Examples of commercially available starting materials with fluorine atoms in these locations are shown in **Figure 2.2**. The final product should have multiple chemically equivalent fluorines in the ligand.

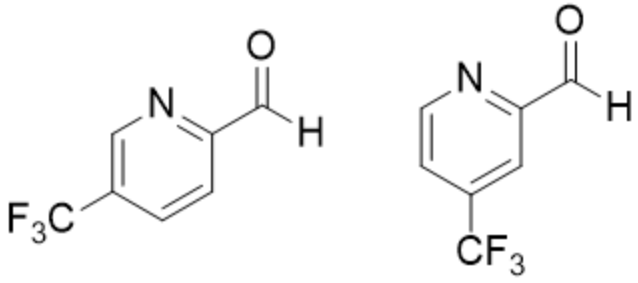

Figure 2.2. Examples of compounds that could be used in synthesis of fluorinated H_2qp1 and other fluorinated quinol- containing ligands.

The first step towards synthesizing fluorinated H_2qp1 was reacting 5-fluoro-2-formylpyridine (**Figure 2.3**) with 1,2-ethanediamine. Adding three equiv. of the fluorinated pyridine yields FTris, which has three installed fluorine atoms. This can then react with 2,5-dihydroxybenzaldehyde to yield the final target F_3H_2qp1. Once produced and characterized, this

fluorinated ligand was to be complexed to an Fe(II) species with either a triflate or perchlorate counteranion.[10,27,29]

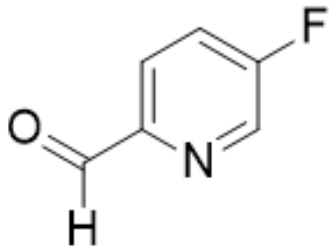

Figure 2.3. Chemical structure of 5-fluoro-2-formylpyridine.

Due to time constraints, I was unable to synthesize the full F_3H_2qp1 ligand but was able to obtain a pure sample of its immediate precursor FTris (**Scheme 2.3**). This ligand could potentially serve as the organic component in a bimodal MRI sensor, so I attempted to complex it to Fe(II). The reaction between FTris and $Fe^{II}(ClO_4)_2$ yielded a sticky red material that was not sufficiently pure to move forward to additional characterization. The use of more rigorously dried solvents may improve the quality of the product. A preliminary ^{19}F NMR spectrum suggests that the complex is paramagnetic (**Figure S4**).

The compound did not appear to be sensitive to air. When a sample of the impure product in MeCN was exposed to air, the UV/vis spectrum did not significantly change over 4.5 h (**Figure S5**), suggesting that the material was not getting oxidized by air. Although this was not rigorously assessed, small bands past 500 nm have the energies and intensities of d-d transitions. High-spin Fe(III) compounds lack such features, suggesting that the impure product contains at least some Fe(II).

2.4. Conclusions

This project aimed to extend the laboratory's prior successes in redox-responsive MRI contrast agents to bimodal sensors with ^{1}H and ^{19}F MRI outputs. The FTris ligand and the proposed F_3H_2qp1 could coordinate to Fe(II) to yield species that are ^{19}F MRI active and ^{1}H MRI silent. The ferrous species could then get oxidized by H_2O_2 or another reactive oxygen species to yield Fe(III) complexes that are ^{1}H MRI active and have a different ^{19}F MRI profile. Future steps for this project are to refine the syntheses of the ligands and Fe(II) complexes, characterize the aqueous speciation and stabilities of the iron compounds, spectroscopically characterize their reactivity with H_2O_2, and assess their MRI properties both before and after oxidation.

2.5. References for Chapters 1 and 2

(1) Grover, V. P. B.; Tognarelli, J. M.; Crossey, M. M. E.; Cox, I. J.; Taylor-Robinson, S. D.; McPhail, M. J. W. Magnetic Resonance Imaging: Principles and Techniques: Lessons for Clinicians. *J. Clin. Exp. Hepatol.* **2015**, *5* (3), 246–255.

(2) Thorat, N. D.; Tofail, S. A. M.; von Rechenberg, B.; Townley, H.; Brennan, G.; Silien, C.; Yadav, H. M.; Steffen, T.; Bauer, J. Physically Stimulated Nanotheranostics for next Generation Cancer Therapy: Focus on Magnetic and Light Stimulations. *Appl. Phys. Rev.* **2019**, *6* (4), 041306.

(3) Westbrook C, Roth CK, Talbot J. *MRI in Practice.* 4th edition London: John Wiley & Sons, Inc.; 2011.

(4) Lohrke, J.; Frenzel, T.; Endrikat, J.; Alves, F. C.; Grist, T. M.; Law, M.; Lee, J. M.; Leiner, T.; Li, K.-C.; Nikolaou, K.; Prince, M. R.; Schild, H. H.; Weinreb, J. C.; Yoshikawa, K.; Pietsch, H. 25 Years of Contrast-Enhanced MRI: Developments, Current Challenges and Future Perspectives. *Adv. Ther.* **2016**, *33* (1), 1–28.

(5) Karbalaei, S.; Goldsmith, C. R. Recent Advances in the Preclinical Development of Responsive MRI Contrast Agents Capable of Detecting Hydrogen Peroxide. *J. Inorg. Biochem.* **2022**, *230*, 111763.

(6) Caravan, P.; Ellison, J. J.; McMurry, T. J.; Lauffer, R. B. Gadolinium(III) Chelates as MRI Contrast Agents: Structure, Dynamics, and Applications. *Chem. Rev.* **1999**, *99* (9), 2293–2352.

(7) Mastrogiacomo, S.; Dou, W.; Jansen, J. A.; Walboomers, X. F. Magnetic Resonance Imaging of Hard Tissues and Hard Tissue Engineered Bio-Substitutes. *Mol. Imaging Biol.* **2019**, *21* (6), 1003–1019.

(8) Gulani, V.; Calamante, F.; Shellock, F. G.; Kanal, E.; Reeder, S. B. Gadolinium Deposition in the Brain: Summary of Evidence and Recommendations. *Lancet Neurol.* **2017**, *16* (7), 564–570.
(9) Sun Zhou, X. D.; Marzke, R.; Peng, Z.; Szilágyi, I.; Dey, S. K. Understanding the High Longitudinal Relaxivity of Gd(DTPA)-Intercalated (Zn,Al)-Layered Double Hydroxide Nanoparticles. *Inorg. Chem.* **2019**, *58* (18), 12112–12121.
(10) Yu, M.; Ward, M.; Franke, A.; Ambrose, S.; Whaley, Z.; Bradford, T.; Gorden, J.; Beyers, R.; Cattley, R.; Ivanović-Burmazović, I.; Schwartz, D.; Goldsmith, C. R. Adding a Second Quinol to a Redox-Responsive MRI Contrast Agent Improves Its Relaxivity Response to H_2O_2. *Inorg. Chem.* **2017**, *56* (5), 2812-2826.
(11) Loving, G. S.; Mukherjee, S.; Caravan, P. Redox-Activated Manganese-Based MR Contrast Agent. *J. Am. Chem. Soc.* **2013**, *135* (12), 4620–4623.
(12) Shokrollahi, H. Contrast Agents for MRI. *Mater. Sci. Eng. C Mater. Biol. Appl.* **2013**, *33* (8), 4485–4497.
(13) Xue, S.; Yang, H.; Qiao, J.; Pu, F.; Jiang, J.; Hubbard, K.; Hekmatyar, K.; Langley, J.; Salarian, M.; Long, R. C.; Bryant, R. G.; Hu, X. P.; Grossniklaus, H. E.; Liu, Z.-R.; Yang, J. J. Protein MRI Contrast Agent with Unprecedented Metal Selectivity and Sensitivity for Liver Cancer Imaging. *Proc. Natl. Acad. Sci. U. S. A.* **2015**, *112* (21), 6607–6612.
(14) Raymond, K. N.; Pierre, V. C. Next Generation, High Relaxivity Gadolinium MRI Agents. *Bioconjugate Chem.* **2005**, *16* (1), 3–8.
(15) Borel, A.; Bean, J. F.; Clarkson, R. B.; Helm, L.; Moriggi, L.; Sherry, A. D.; Woods, M. Towards the Rational Design of MRI Contrast Agents: Electron Spin Relaxation Is Largely Unaffected by the Coordination Geometry of Gadolinium(III)-DOTA-Type Complexes. *Chem.* **2008**, *14* (9), 2658–2667.
(16) Čolak, E.; Žorić, L. 6 - Antioxidants and Age-Related Macular Degeneration. In *Handbook of Nutrition, Diet, and the Eye (Second Edition)*; Preedy, V. R., Watson, R. R., Eds.; Academic Press, 2019; pp 85–106.
(17) Leslie, J. B.; Raffa, R. B.; Jr, R. T.; Tabor, A.; Muniz, E.; Nalamachu, S.; Jr, J. V. P. Essential Oxygen Oil for Treatment of Sport-Related Injuries. *Am. J. Sports Med.* **2013**, *1* (1), 7–12.
(18) Tönnies, E.; Trushina, E. Oxidative Stress, Synaptic Dysfunction, and Alzheimer's Disease. *J. Alzheimers Dis.* **2017**, *57* (4), 1105–1121.
(19) Lee Mosley, R.; Benner, E. J.; Kadiu, I.; Thomas, M.; Boska, M. D.; Hasan, K.; Laurie, C.; Gendelman, H. E. Neuroinflammation, Oxidative Stress, and the Pathogenesis of Parkinson's Disease. *Neurol. Clin. Neurosci.***2006**, *6* (5), 261–281.
(20) Gale, E. M.; Mukherjee, S.; Liu, C.; Loving, G. S.; Caravan, P. Structure–Redox–Relaxivity Relationships for Redox Responsive Manganese-Based Magnetic Resonance Imaging Probes. *Inorg. Chem.* **2014**, *53* (19), 10748–10761.
(21) Bonnet, C. S.; Tóth, É. Smart Contrast Agents for Magnetic Resonance Imaging. *CHIMIA.* **2016**, *70* (1–2), 102.
(22) Wang, H.; Jordan, V. C.; Ramsay, I. A.; Sojoodi, M.; Fuchs, B. C.; Tanabe, K. K.; Caravan, P.; Gale, E. M. Molecular Magnetic Resonance Imaging Using a Redox-Active Iron Complex. *J. Am. Chem. Soc.* **2019**, *141* (14), 5916–5925.
(23) Peterson, K. L.; Srivastava, K.; Pierre, V. C. Fluorinated Paramagnetic Complexes: Sensitive and Responsive Probes for Magnetic Resonance Spectroscopy and Imaging. *Front. Chem.* **2018**, *6*, 160.

(24) Srivastava, K.; Ferrauto, G.; Young, V. G.; Aime, S.; Pierre, V. C. Eight-Coordinate, Stable Fe(II) Complex as a Dual ^{19}F and CEST Contrast Agent for Ratiometric pH Imaging. *Inorg. Chem.* **2017**, *56* (20), 12206–12213.
(25) Srivastava, K.; Weitz, E. A.; Peterson, K. L.; Marjańska, M.; Pierre, V. C. Fe- and Ln-DOTAm-F12 Are Effective Paramagnetic Fluorine Contrast Agents for MRI in Water and Blood. *Inorg. Chem.* **2017**, *56* (3), 1546–1557.
(26) Meng, Q.; Wu, M.; Shang, Z.; Zhang, Z.; Zhang, R. Responsive Gadolinium(III) Complex-Based Small Molecule Magnetic Resonance Imaging Probes: Design, Mechanism and Application. *Coord. Chem. Rev.* **2022**, *457*, 214398.
(27) Yu M., Ambrose S. L., Whaley Z. L., Fan S., Gorden J. D., Beyers R. J., Schwartz D. D., Goldsmith C. R. A Mononuclear Manganese(II) Complex Demonstrates a Strategy to Simultaneously Image and Treat Oxidative Stress. *J. Am. Chem. Soc.*, **2014**, *136*, 12836-12839.
(28) Ward M. B., Scheitler A., Yu M., Senft L., Zillmann A. S., Gorden J. D., Schwartz D. D., Ivanović-Burmazović I., Goldsmith C. R. Superoxide Dismutase Activity Enabled by a Redox-Active Ligand rather than a Metal. *Nat. Chem.* **2018**, *10*, 1207-1212.
(29) Giorgio, M.; Trinei, M.; Migliaccio, E.; Pelicci, P. G. Hydrogen Peroxide: A Metabolic by-Product or a Common Mediator of Ageing Signals? *Nat. Rev. Mol. Cell. Biol.* **2007**, *8* (9), 722–728.

Appendix 1: Supplemental Information

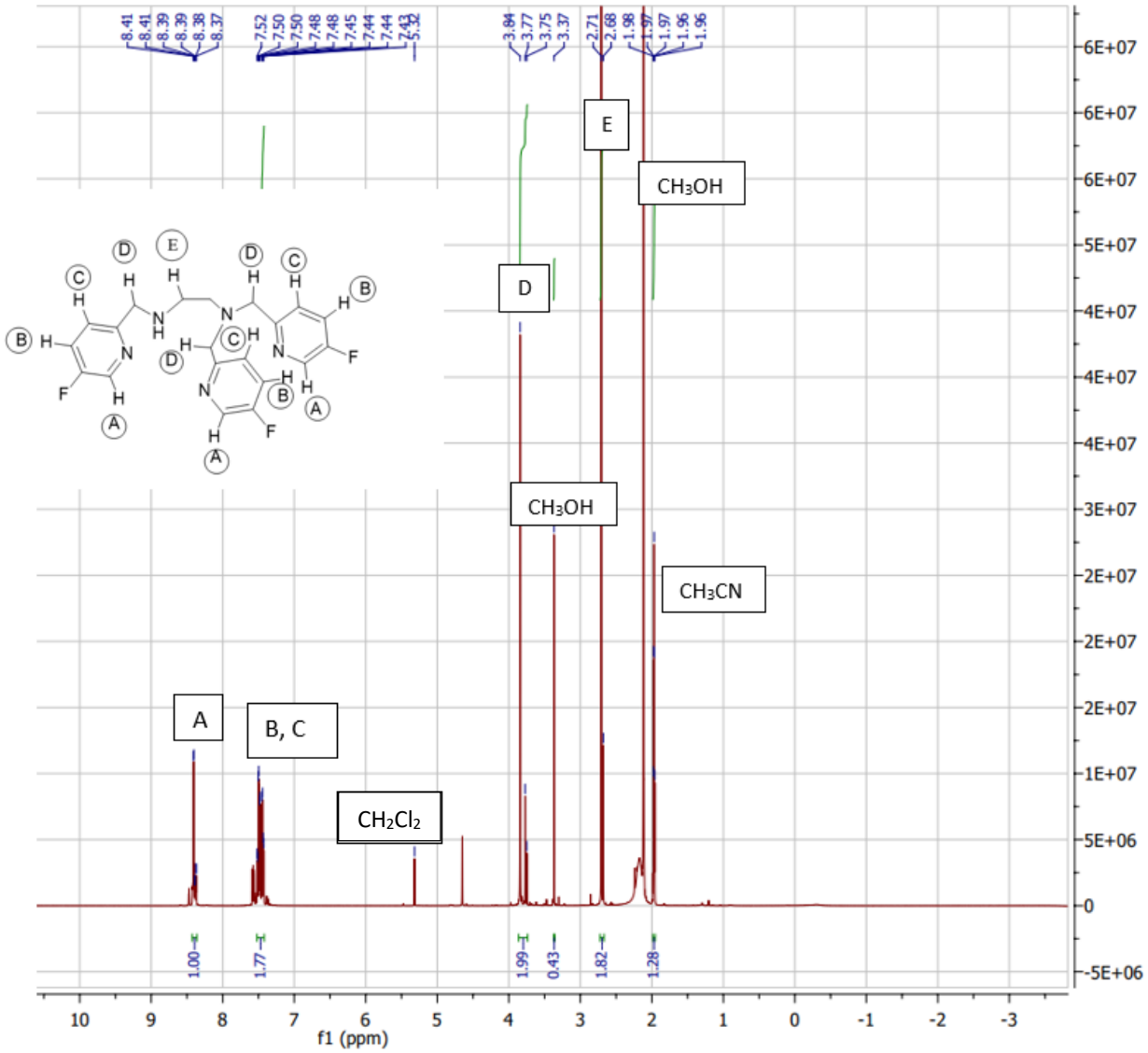

Figure S1. ^{1}H NMR spectrum of fluorinated trispicen (FTris). ^{1}H NMR (500 MHz, MeCN-d_3, 293 K): δ 8.41 (m, 3H), 7.52-7.43 (m, 6H), 3.77 (s, 6H), 2.71 (s, 4H)

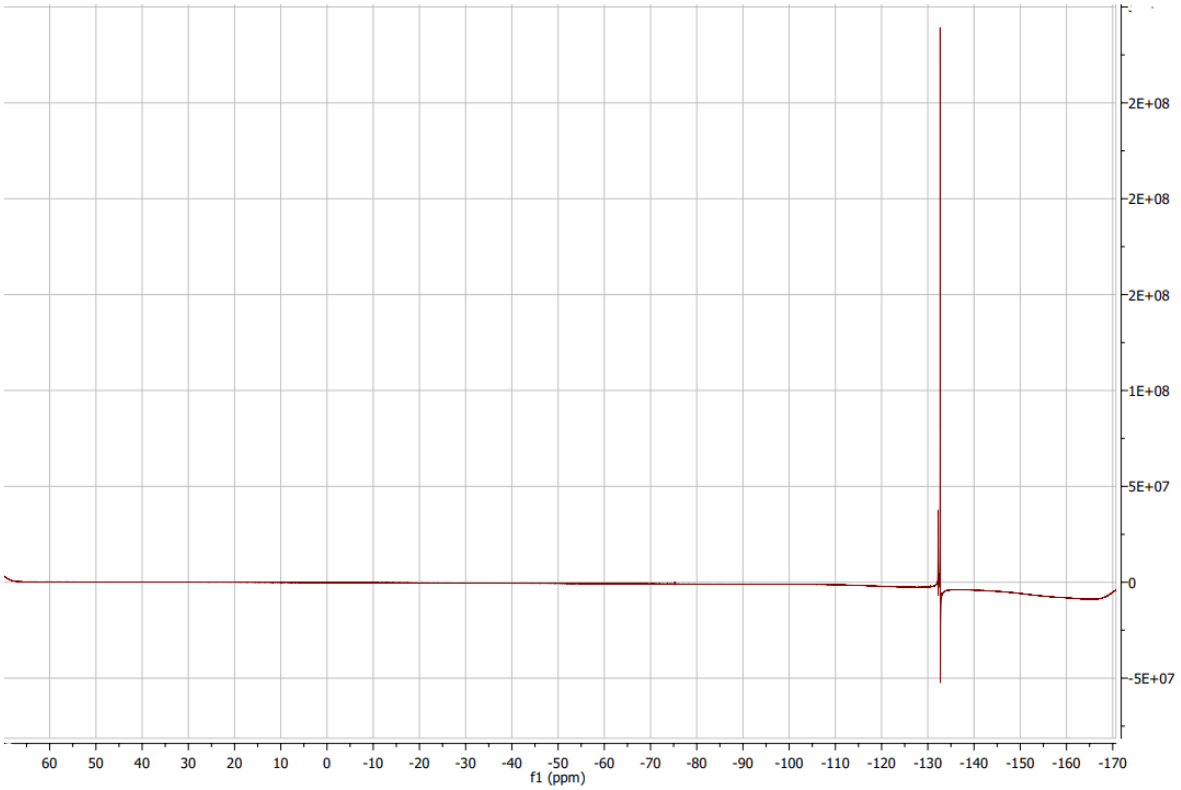

Figure S2. ^{19}F NMR of fluorinated trispicen (FTris) taken in MeCN-d_3 on a 500 MHz NMR spectrometer at 294 K. Zinc(II) trifluoromethanesulfonate was used as reference peak.

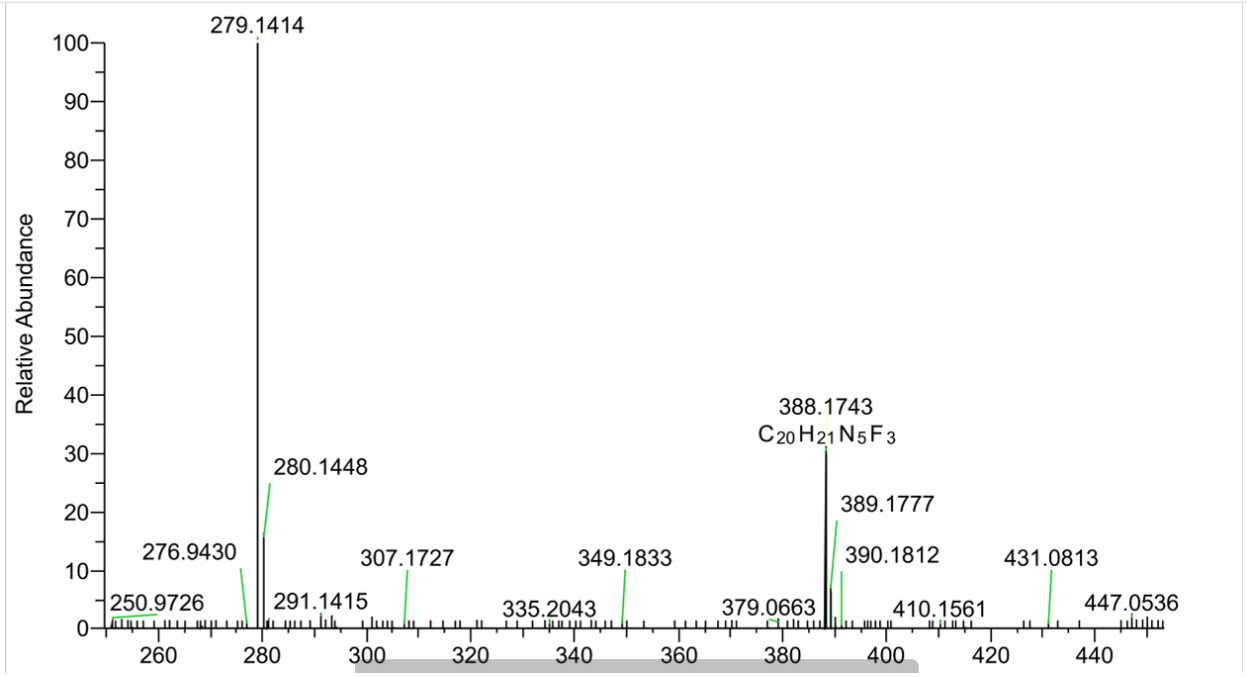

Figure S3. Mass spectrometry data for FTris. Calculated m/z = 388.1743. Observed m/z = 388.1743.

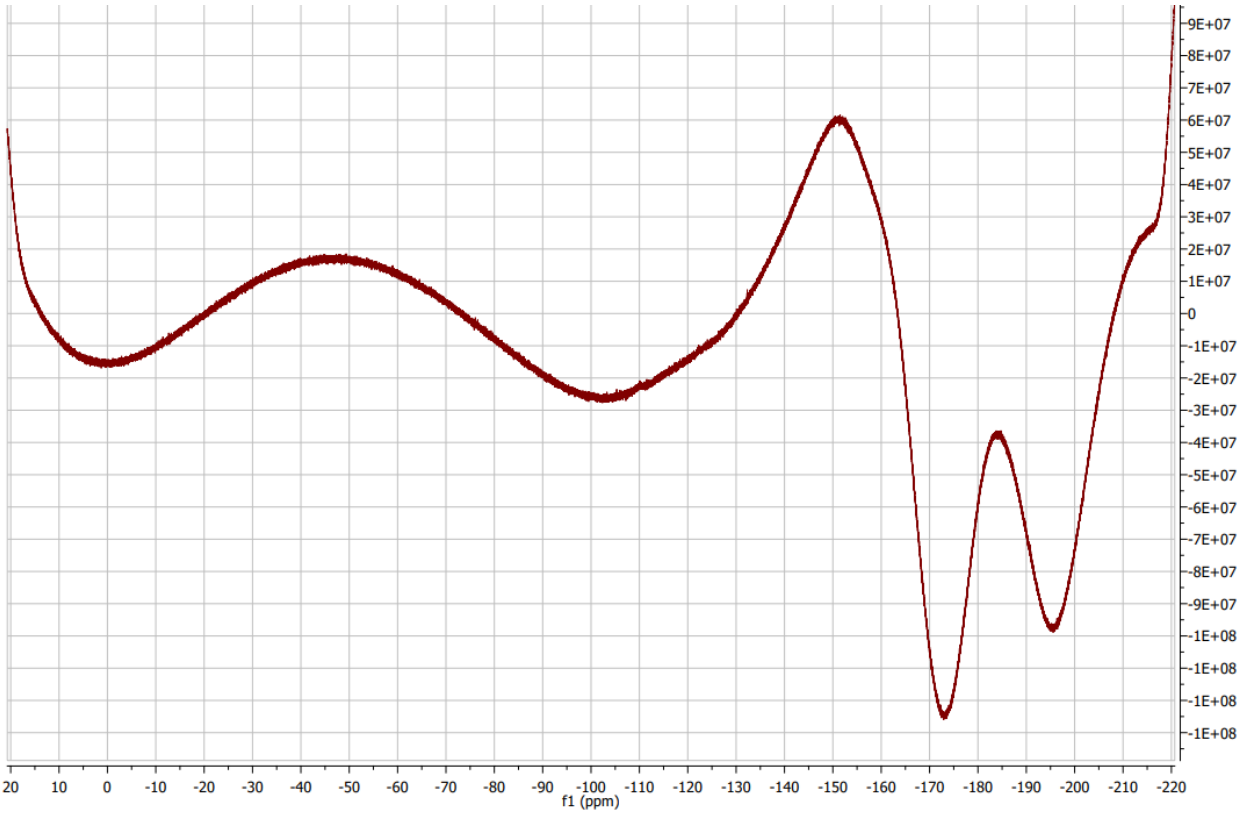

Figure S4. ^{19}F NMR spectrum of $[Fe^{II}(Ftris)(ClO_4)_2]$ taken in MeCN-d_3. The broad peak at -152 ppm is presumably the main signal with a shoulder at -185 ppm. The bumpy baseline is likely the result of impurities.

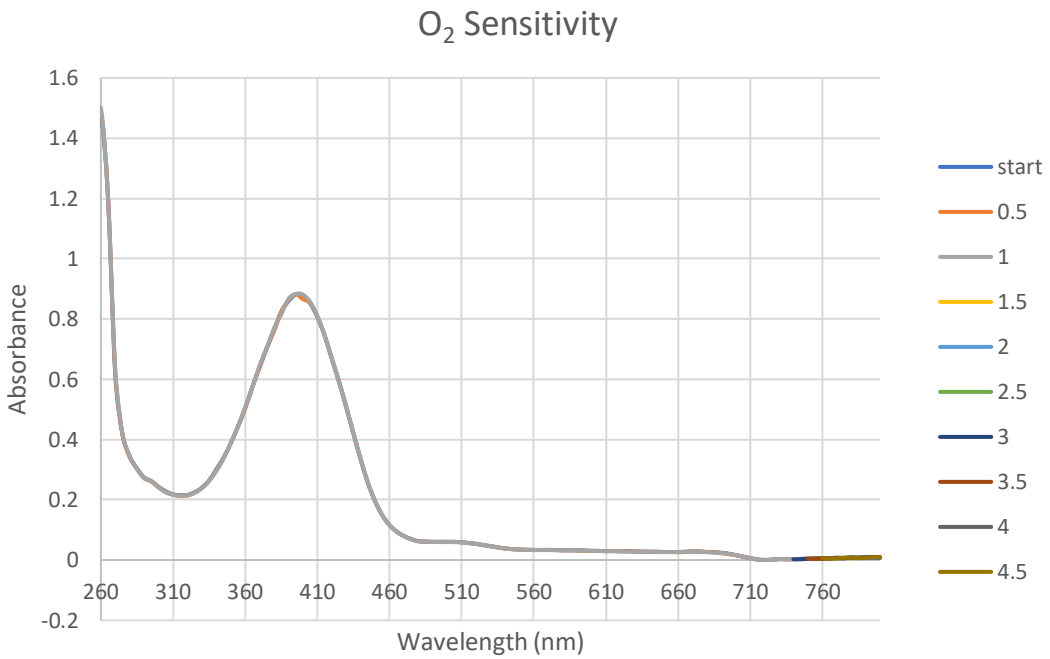

Figure S5. O_2 Sensitivity of $[Fe^{II}(Ftris)(ClO_4)_2]$ taken in MeCN. Scans were taken every half hour. Time points are given in units of h. No oxidation occurred over 4.5 h.

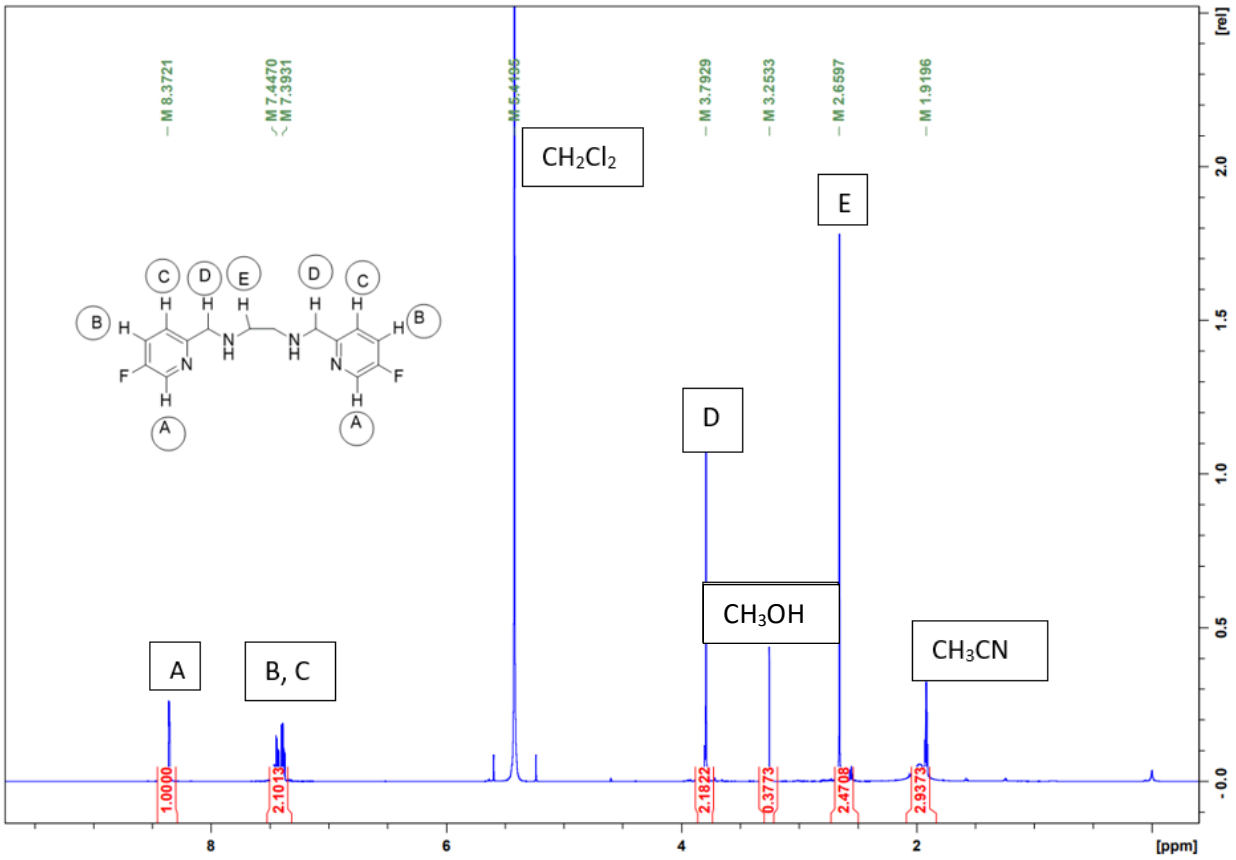

Figure S6. ^{1}H NMR spectrum of fluorinated bispicen **1**. ^{1}H NMR (500 MHz, MeCN-d_3, 293 K): δ 8.37 (qd, J = 5.2 Hz, 1.6 Hz, 0.8 Hz, 2H), 7.44 (dt, J = 9.6 Hz, 2.0 Hz, 2H), 7.39 (m, 4 H), 7.38 (d, J = 1.6 Hz, 4H), 5.41 (m, 2H), 3.79 (s, 4H), 3.25 (s, 4H), 2.65 (s, 4H).

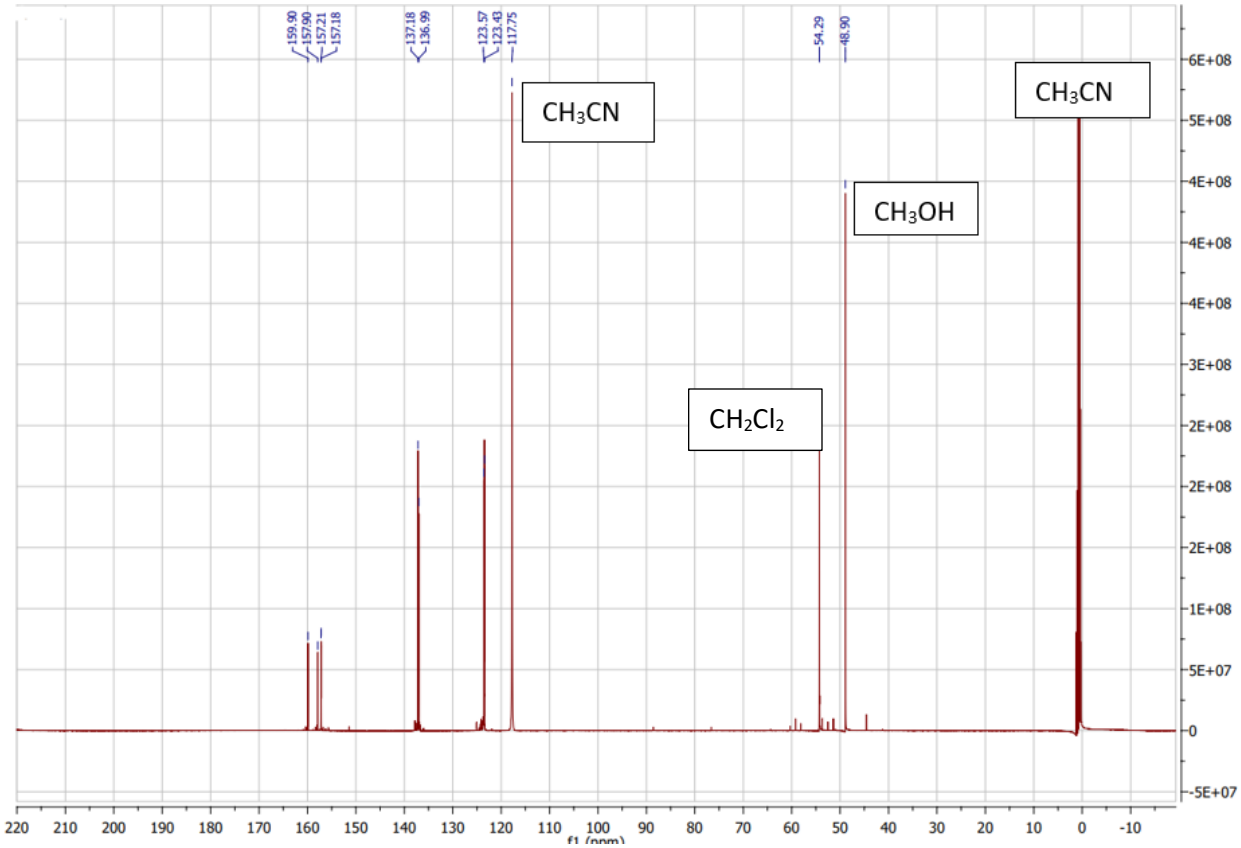

Figure S7. ^{13}C NMR of fluorinated bispicen **1**. 7 peaks expected, 7 peaks observed beyond solvent peaks. ^{13}C NMR (500 MHz, CD_3CN, 293 K): δ 159.90, 157.90, 157.21, 157.18, 137.18, 136.99, 123.57, 123.43, 118.20, 54.29, 48.90, 1.30.

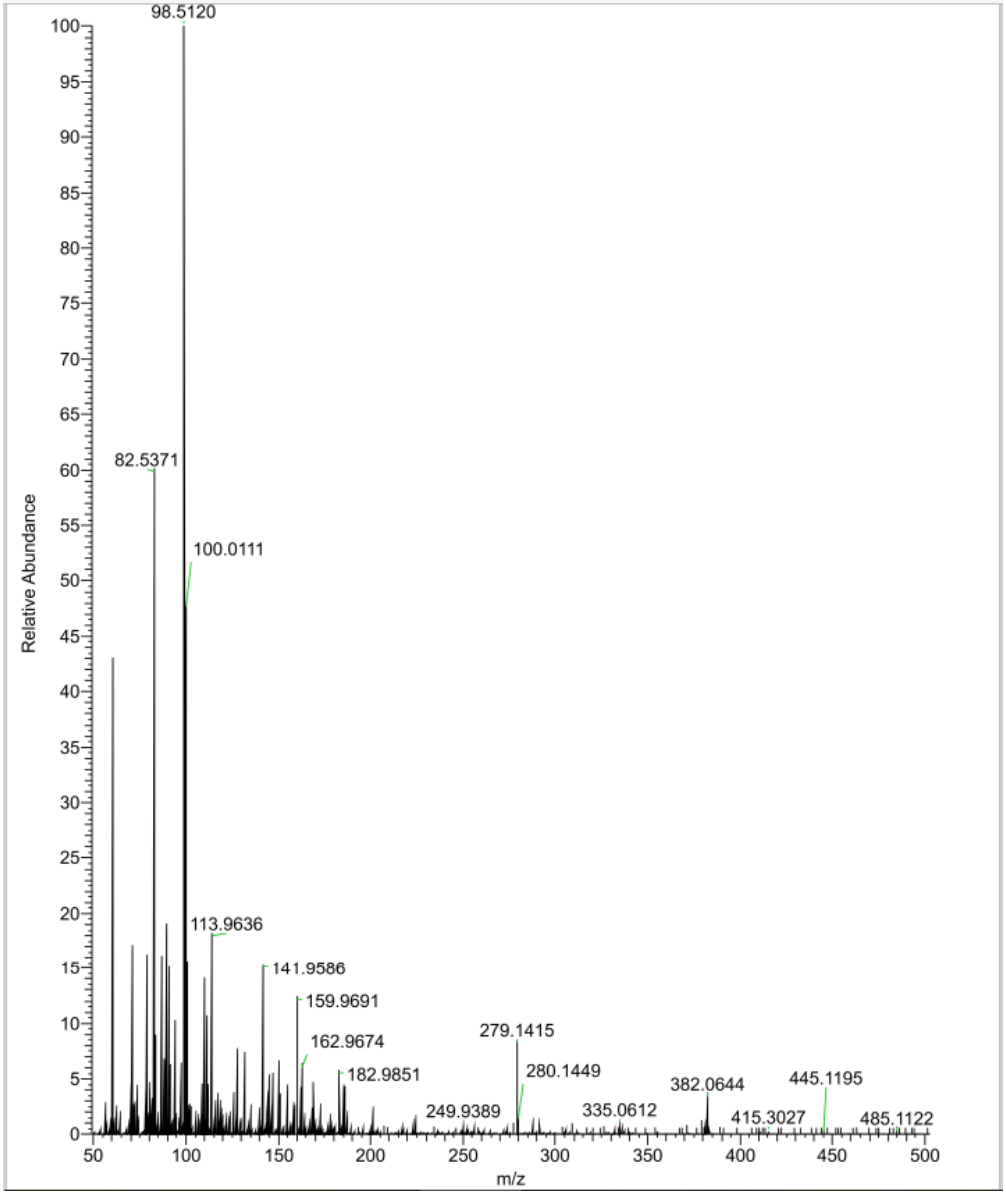

Figure S8. Mass Spectrometry data for fluorinated bispicen **1**. $C_{14}H_{16}N_4F_2$ protonates to $C_{14}H_{17}N_4F_2^+$. Calculated m/z = 279.1421. Observed m/z = 279.1415.